NOVATEUR PUBLICATIONS
JournalNX- A Multidisciplinary Peer Reviewed Journal
ISSN No: 2581-4230
VOLUME 3, ISSUE 12, Dec. -2017

LOW HEAD PICO HYDRO UNIT USING LOW COST INDUCTION MOTOR AND WATER WHEEL

S.S.KATRE
shrikantkatre@gmail.com

ABSTRACT:

This paper presents a case study of employing a water wheel and a self excited induction generator combination for a Pico hydro generation unit. Simple procedure of designing a high speed water wheel is presented. A prototype Pico hydro generation unit is fabricated by authors. The unit was tested at actual site of low head water flow. Laboratory test results, on site test results and simulation results are presented.

A remarkable agreement is observed between the laboratory and site tests. MATLAB simulation corroborates the field and laboratory findings. A check dam across a river in district Sangli of the state of Maharashtra, India is chosen for the field trials. The effective water head available round the year is 1 meter. Water discharge data has been obtained from the Department of Irrigation, State of Maharashtra.

KEY WORDS: Induction generator, magnetizing reactance, excitation, capacitor, water wheel, Pico-hydro generation, etc.

I. INTRODUCTION:

Energy crisis has been the catchy phrase over past couple of decades. Researchers have been devoting significant attention to developing clean means of energy generation. Of all the non-renewable energy resources, the thermal generation has been sharing major chunk in the world production of energy. On the other hand, solar and wind generation technologies have undergone mind-blowing evolution and have come to a stage of tangible applications though at somewhat higher initial costs. The third major option in the renewable energy sector is micro and Pico-hydro generation. The Pico-hydro category is classified as those units which generate less than 5 Kilowatt of electrical power. Water flows with head as low as 1 meter and running round-the-year are found in thousands, across the terrains of every country. This seemingly huge potential is still untapped. Among around 2000 check dams available in the state of Maharashtra, Pico-Hydro plants are hardly found anywhere. Moreover, application of Pico-hydro technology does not necessarily require a check dam structure. It can be deployed by channeling the water flow where there is an available head. These small power plants are suitable for distributed generation [1]. Water flows with low head are also available at many places such as the water supplied to the consumers [2]. For large power generation applications, alternators are used and for low power generation, low-cost induction generators are used. They are gaining popularity in the renewable sector due to simple construction, minimum maintenance and low cost. Haval Sardar Kamil and S. U. Kulkarni (2013), discussed the application of wound rotor and squirrel cage induction motors as induction generators for electrical power generation [3]. The generation starts at much lower speeds than the synchronous speed of the machine. Pico-hydro generating plants can make use of these types of induction generators in isolated self excited induction generator (SEIG) mode.

The cost of Pico-hydro power generating units is low. They are simple in construction and do not require highly skilled personnel for their operation and maintenance. Induction generators possess a peculiar feature that they stop generation when they are overloaded, without any side-effects. Thus, separate overload protection is not necessary. Fabrication and installation time for these units is also very short. Working of such induction generators is discussed briefly in the next section.

II. ISOLATED SELF EXCITED INDUCTION GENERATOR (SEIG):

Induction generators find applications both in Pico-Hydro generation and in higher capacities of generating plants. Pico-hydro units are invariably operated in isolated mode and not in the power grid. In the Pico-hydro applications, squirrel cage type induction motors are most commonly used as self excited induction generators. In the isolated self-excited mode, required reactive power is supplied through capacitors connected across motor windings. Squirrel cage induction motors are robust and economical. For self-excitation to occur, it is essential that residual flux is present in the machine. To ensure voltage build-up, capacitors of appropriate value need to be connected across motor windings and the motor is to be driven above a certain minimum speed [4]. Phasor diagram in Fig. 1 shows how the voltage build-up is achieved by connecting capacitors across motor windings. E_1 is the induced emf and V_t is the stator terminal voltage. Stator current I_s at no load is same as capacitor current I_c it leads V_t by 90^0. Magnetizing component I_m of stator current is in phase with the flux. It helps in flux build up,

which results in an increase in the induced emf. This rise in the emf continues till a steady state is reached.

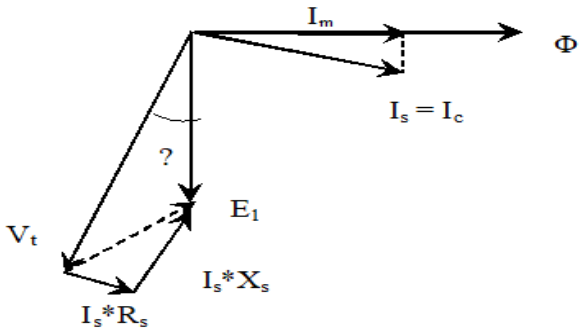

Fig. 1 Phasor diagram of SEIG at no load with capacitor connected across stator winding

Theodore Wildi (2002), Ofualagba G. and Ubeku E. U. (2011), suggested per phase, per unit equivalent circuit at the base frequency for steady state analysis of a self-excited induction generator as shown in fig. 2. It is assumed that core loss is negligible as it is very low in magnitude, the magnetizing reactance is only affected due to saturation and all the other parameters remain constant [5-6].

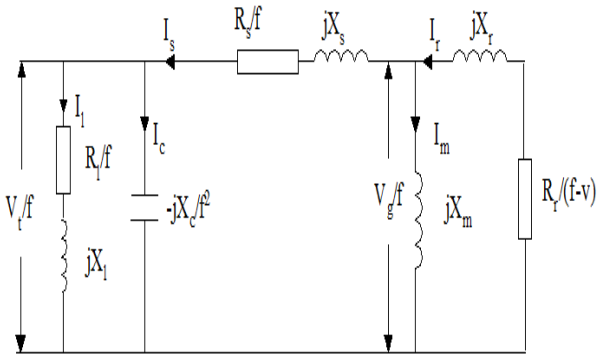

Fig. 2 Per unit, per phase equivalent circuit of an SEIG at base frequency

Where

R_s, R_r, R_l: P. u. per phase Stator, rotor and load resistances respectively.

X_s, X_r , X_m , X_l : P.u. per phase Stator leakage, rotor leakage, magnetizing and load reactance at base frequency respectively.

I_s , I_r , I_c , I_l: P. u. per phase stator, rotor, capacitor and load current respectively.

f_b : Base or main supply frequency (Hz).

f_a : Actual frequency of generated voltage.

f : P. u. frequency = f_a/f_b

N_s: Synchronous speed of the machine (rpm).

N_a: Actual speed of the machine (rpm).

v: p. u. speed = N_a / N_s

V_g: Air gap voltage or voltage across magnetizing reactance.

V_t : Terminal voltage

Using loop current method, at steady state

$$I_s(Z_1 + Z_2) = 0 \quad (1)$$

Where

Z_1 is the impedance of load and capacitor combination

Z_2 is the impedance of induction generator

Z_t is the total impedance of load, capacitor and generator

$$Z_1 + Z_2 = Z_t \quad (2)$$

$$\therefore I_s Z_t = 0 \quad (3)$$

When the generator excites, $I_s \neq 0$

$$\therefore Z_t = 0 \quad (4)$$

This means that the real part and imaginary part of the total impedance is zero. Following equations can be derived.

$$R_1 = \frac{R_s}{f} + \frac{X_m^2 R_r (f - v)}{R_r^2 + (f - v)^2 (X_r + X_m)^2} \quad (5)$$

$$R_2 = \frac{R_l X_c^2 / f}{R_l^2 f^2 + (f^2 X_l - X_c)^2} \quad (6)$$

$$X_1 = X_s + X_m \frac{R_r^2 + X_r (f - v)^2 (X_r + X_m)}{R_r^2 + (f - v)^2 (X_r + X_m)^2} \quad (7)$$

$$X_2 = (-X_c) \frac{R_l^2 + X_l (X_l f^2 - X_c)}{R_l f^2 + (f^2 X_l - X_c)^2} \quad (8)$$

Here, R_1 and R_2 are the real parts of generator impedance and combined load-capacitor impedance respectively. X_1 and X_2 are imaginary parts of generator and load and capacitor impedances respectively.

III. DETERMINATION OF EQUIVALENT CIRCUIT PARAMETERS:

TESTING OF INDUCTION MOTOR:

Constant and variable losses, rotor resistance, stator and rotor leakage reactance of the motor are estimated from no load and blocked rotor tests. The specifications of the motor are Kirloskar make, three phase, 2.2 KW, 415 V, 4.5 A, 1440 rpm, squirrel cage, delta connected motor. Table-1 and Table-2 show no load and blocked rotor test readings respectively.

Table1: No load test readings

V_o (V)	I_o (A)	W_o (W)
415	1.9	440

Table2: Blocked rotor test readings

V_{sc} (V)	I_{sc} (A)	W_{sc} (W)
134	4.5 (Line)	550

From no load test following parameters are obtained

$$cos\varphi_0 = 0.322 \quad (9)$$

$$X_{max} = 399.8\,\Omega \quad (10)$$

From blocked rotor test following parameters are obtained

$Cos\varphi_{sc}$= 0.526 (11)

Rotor resistance =15.46 Ω

Stator winding resistance = 11.7 Ω (Measured)

Stator leakage reactance = 21.91 Ω

Rotor leakage reactance = 21.91 Ω
Stator winding impedance = 24.83 Ω

Magnetizing reactance X_m is calculated for different input voltages by conducting a synchronous speed test. The rotor is driven at synchronous speed by a prime mover. There is no rotor copper and iron loss. The rotor circuit is eliminated from the equivalent circuit. The voltage across magnetizing reactance is calculated by subtracting the stator impedance drop from the input voltage. Table-3 shows magnetizing reactance test readings.

Table 3 Magnetizing reactance test readings

Input voltage (V)	Input Line current (A)	Stator voltage drop (V)	Air-gap voltage V_g	Magnetizing Reactance X_m (Ohms)	V_g/f p.u.	X_m p.u.
50	0.26	3.72	46.28	308.29	0.111	1.93
98	0.5	7.16	90.16	314.67	0.217	1.97
145.6	0.75	10.75	134.86	311.44	0.325	1.95
190	1.0	14.33	175.67	304.26	0.423	1.90
250	1.4	20	230.00	284.54	0.554	1.78
300	1.8	25.80	274.20	263.84	0.66	1.65
350	2.42	34.69	315.30	225.66	0.76	1.41
400	3.15	45.16	354.84	195.10	0.855	1.22
415	3.88	55.60	359.4	160.43	0.866	1.00

Fig. 3 shows a plot of p. u. V_g/f Vs p. u. X_m.

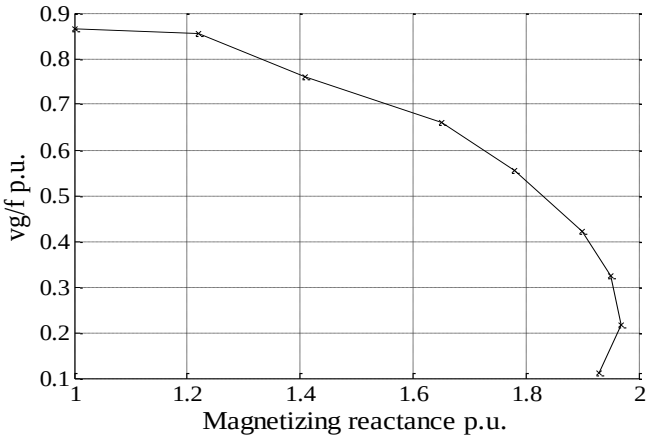

Fig. 3 Variation of Vg/f p. u. with p. u. Xm

The magnetizing reactance X_m is nonlinear. From the substantially linear portion of the curve, an approximately linear relationship between V_g and X_m is obtained using curve fitting tool in MATLAB and the relation is

$$\frac{V_g}{f}\ p.u. = 1.7 - 0.7X_m \quad (15)$$

Fig. 4 shows the magnetization curve for the machine. Here, $X_m = V_g/I_m$ is the slope of the line drawn from the origin and intersecting the curve. Tangent to the curve gives the value of maximum magnetizing reactance X_{max}. The machine will excite as long as the value of X_m is less than X_{max}. The point of intersection of the curve and the magnetizing reactance line gives the steady state voltage V_g, the generator will develop for a given value of X_m.

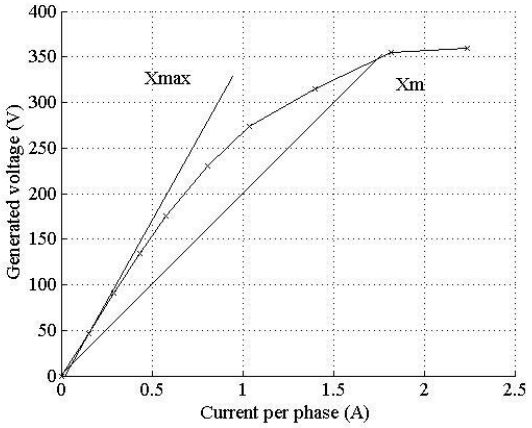

Fig. 4 Magnetization curve for the motor

Fig. 5 shows the phasor diagram of an isolated self-excited induction generator. Line A-C represents terminal voltage V_t. Capacitor current is shown by line A-I_c. Load current I_l lags V_t as the inductive load is assumed. Line A-I_s represents stator current. Stator impedance drop $Z_s * I_s$ is added to V_t and shown by line C-B. Line A-B represents V_g, air gap voltage. Line B-D is drawn perpendicular to line A-C.

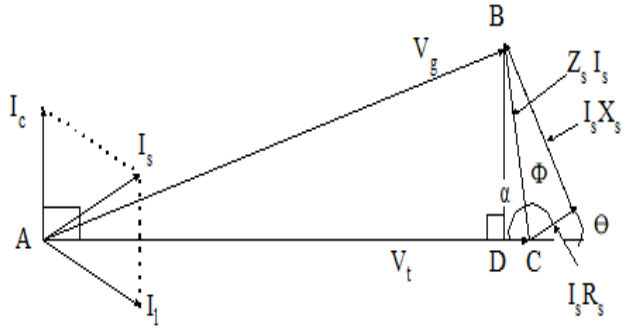

Fig.5 Phasor diagram of an isolated SEIG

From triangle ABC

$$AB^2 = (AC - DC)^2 + BD^2 \quad (16)$$

$$V_g^2 = V_t^2 + (Z_s I_s)^2 - 2V_t(Z_s I_s)cos\alpha \quad (17)$$

If Z_p is the impedance of parallel branch consisting capacitor and load, then

$$I_s = \frac{V_t}{Z_p} \quad (18)$$

Here, stator current I_S leads the terminal voltage V_t by angle θ, stator impedance angle is Φ and $\angle DCB = \angle\alpha = \angle(180^0 - \theta - \phi)$. Hence, V_t can be calculated, as the values of V_g, Z_s and Z_p are known.

Fig. 6 shows MATLAB simulation of the voltage build-up process in an induction generator.

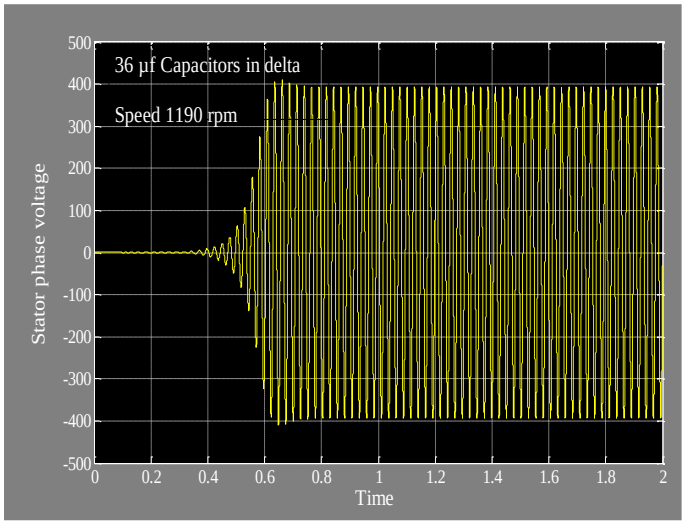

Fig. 6 Voltage build-up in induction generator

Voltage build-up is initiated at about 0.3 seconds after starting the generator. The steady state is reached just after 0.6 seconds. Due to the remnant flux in the rotor small magnitude of emf is induced in the stator. Capacitors provide a path for the stator current. Magnetizing component of the stator current is in phase with the flux so that the flux is strengthened. As a result the induced emf increases. This cumulative process continues till a steady state is reached. Magnetizing inductance also varies during this voltage build-up due to change in the stator current.

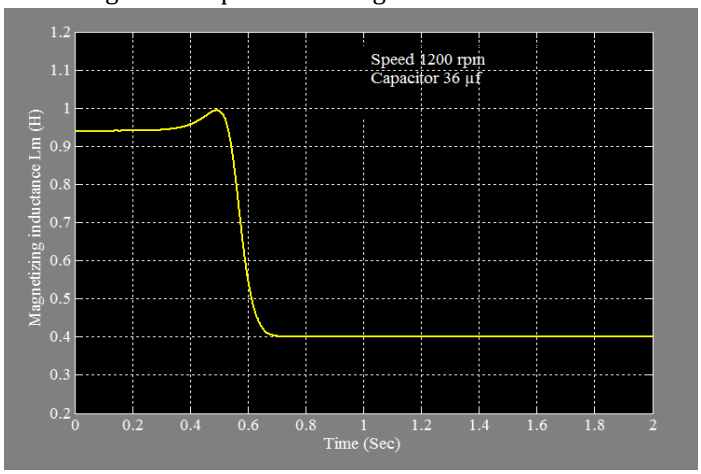

Fig. 7 deviation of magnetizing inductance during voltage build-up

LABORATORY TESTING AS A SELF-EXCITED INDUCTION GENERATOR:

The motor is tested as a self-excited induction generator at no load and on load. Three capacitors of 36 µf each were connected in delta across the motor terminals and no load voltage is measured for different speeds. The second test was conducted by connecting three capacitors of 80 µf each in delta across the motor terminals. Fig. 8 shows the test setup with instruments, capacitors and load.

Fig. 8 Test setup

Table-4 shows readings of speed and generated voltage for 36 µf capacitors and table -5 shows readings for 80 µf capacitors. Comparison between actual readings and simulation results in MATLAB for both cases at no load are shown in fig.9 and fig. 10.

Table 4 Speed and output voltage for 36 µf capacitors

Speed (RPM)	Output Voltage
1190	415
1153	390
1098	350
1067	320
1026	285
945	232
920	200
891	160

Table 5 Speed and output voltage for 80 µf capacitors

Speed (RPM)	Output Voltage
980	415
950	382
900	340
850	310
800	265
750	235
700	200
660	160

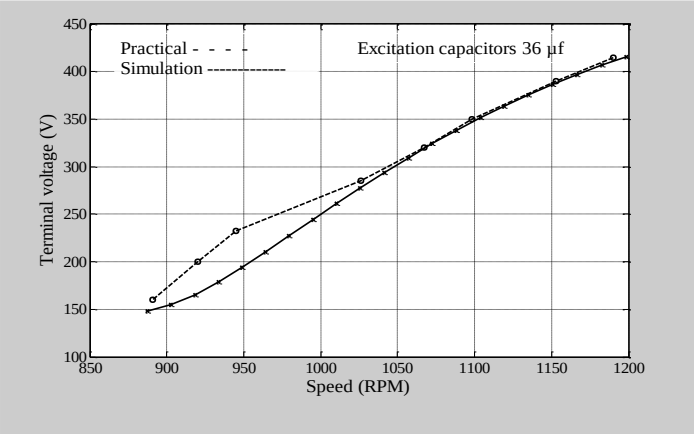

Fig. 9 Practical and simulation results for 36 µf capacitors at no load

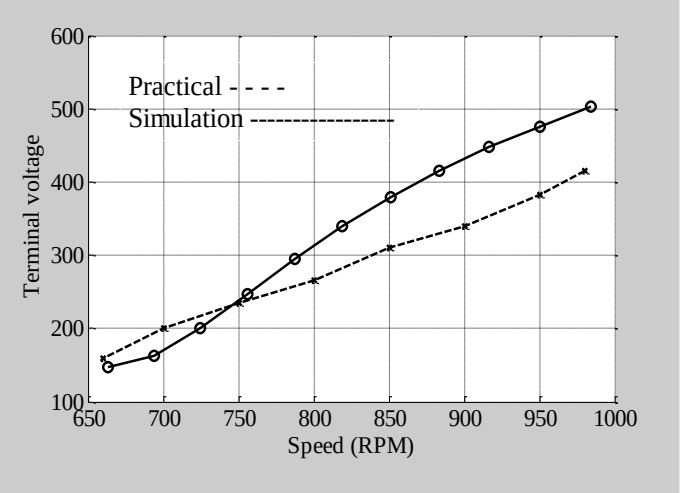

Fig. 10 Practical and simulation results for 80 µf capacitors at no load

A load test is conducted by connecting three capacitors of 80 µf in delta across generator terminals and using resistive load. The terminal voltage was adjusted by adjusting the speed of prime mover for every load. Readings are tabulated in Table-6.

Table 6 Generator readings on load for 80 µf capacitors in delta

Sr. No.	Speed (RPM)	Load (Watts)	Generated voltage
1	750	0	235
2	775	100	238
3	780	200	240
4	805	300	239
5	810	400	235
6	820	500	236
7	835	600	235
8	855	700	224
9	900	800	213

Fig. 11 shows actual and simulation results for the load test.

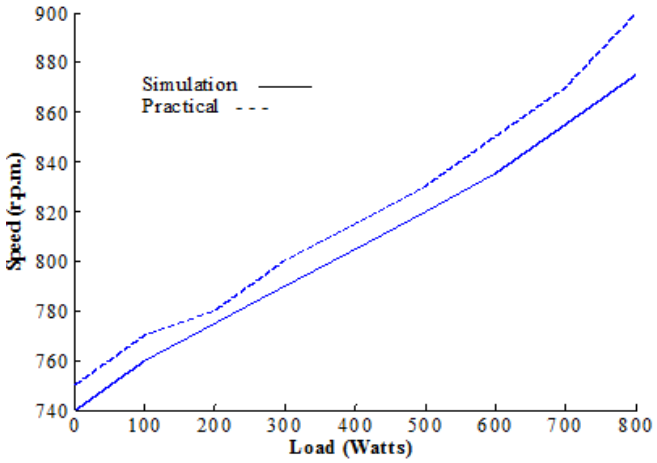

Fig. 11 Simulation and actual results on load

When the value of excitation capacitors across the generator windings is increased, two parameters get affected. The first parameter is the reactive power drawn by the capacitors. As already discussed, for higher value of capacitor, the capacitive reactance is small and for a given voltage the capacitor current increases. The total load on the generator also increases. As this load gets reflected on the prime mover as a mechanical load, the load on the prime mover also increases. Variation of capacitor current with capacitor value is shown for a 3.7 KW motor at no load in fig. 12

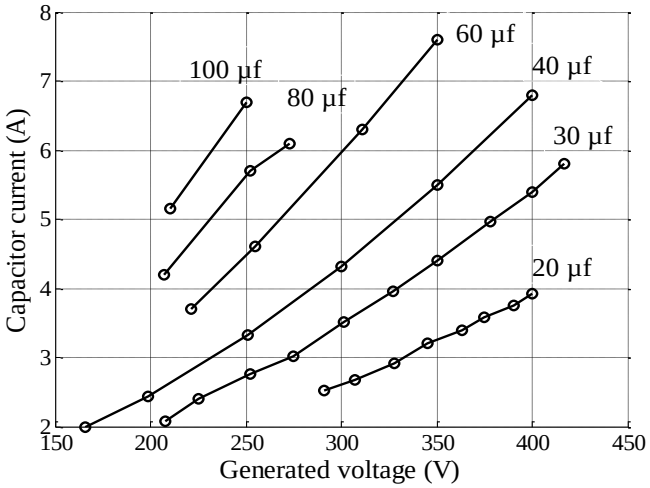

Fig. 12 Capacitor current Vs generated voltage

It is observed that for 250 volts supply the capacitor current varies from 2.5 amperes for 30 µf to 6.5 amperes for 100 µf. Secondly as the generation of voltage starts at lower speeds for high value of excitation capacitors, the frequency of the generated voltage is low hence, low capacitor values are preferred.

Variation of prime mover current with generated voltage at no load is shown in fig. 13.

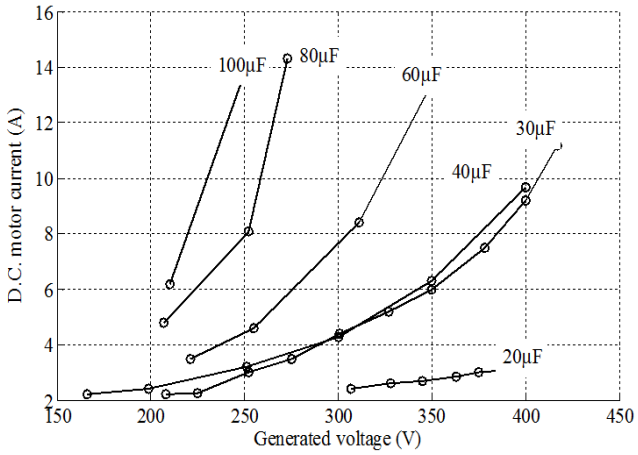

Fig. 13 Prime mover current Vs generated voltage

Due to increase in the excitation capacitor value, the total load on the generator and on the prime mover increases. It can be seen that the d.c. motor is over loaded at no load due to 100 µf capacitor and the generated voltage is just 250 volts.

IV. STEADY STATE ANALYSIS:

Equations (5)-(8), can be solved by specifying any two unknowns out of X_m, v, X_c, f and solving the equations simultaneously. There is always a maximum and a minimum value of capacitor for which the generator can just excite, S.S. Katre et al (2010), [7]. For any value of capacitor smaller than the minimum value, capacitive reactance is high so that the low excitation current does not suffice to build up the flux. The speed at which the generation starts also depends on the capacitor value. For smaller capacitors, higher speed is required. The machine is simulated in MATLAB. Fig. 14 shows the variation of X_m for different values of excitation capacitors. The curves are drawn for purely resistive load with v =1 p. u.

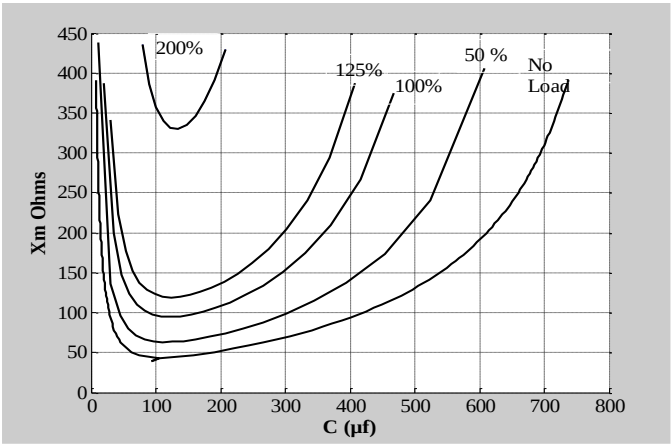

Fig. 14 Variation of Xm with C

The value of X_{max} for the motor is 399.8 ohms. For lower values of excitation capacitor, X_c is high. Excitation capacitor current is low hence magnetizing current is small and generated voltage is low, the value of X_m is high, generation starts at a speed nearly identical to the rated speed. Now if the capacitor value is increased, generated voltage increases and X_m decreases this continues up to a definite value of the capacitor, afterward, the capacitor reactance becomes low and it draws more current causing the terminal voltage to drop. From here, the magnetizing reactance X_m starts increasing again till it reaches X_{max}. As the load increases, the range between the maximum and the minimum value of capacitor becomes narrow. For a small value of excitation capacitor, generation starts at a higher speed as compared to a large value of the capacitor.

Fig.15 shows variations of frequency with change in the terminal capacitor values. The frequency of the generated voltage decreases with increase in capacitor value for a given load. The frequency also decreases for an increase in load for a given value of the capacitor.

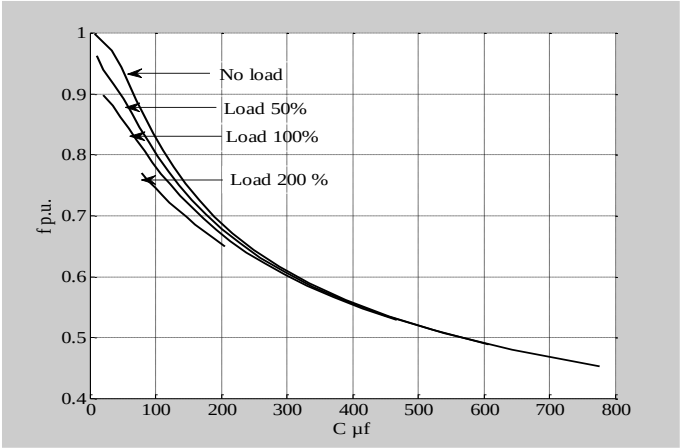

Fig. 15 Variation of frequency with capacitor values

Terminal voltage and air gap voltage also vary with the excitation capacitor values. The relationship between V_g and X_m is given in (9). Fig. 16 shows voltage V_g across magnetizing reactance and voltage V_t across the load, for resistive loads and different values of capacitors.

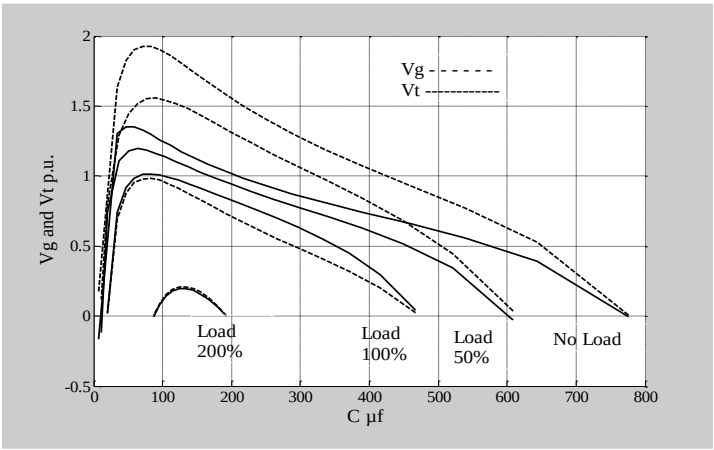

Fig. 16 Variation of Vg and Vt with capacitor values

The terminal voltage may rise above 1.5 p. u. for certain load capacitor combination.

Fig. 17 shows the effect of load power factor on V_g and V_t for different values of excitation capacitors. Here, the load

impedance is taken as 1 p. u. for all cases. All the power factors are lagging.

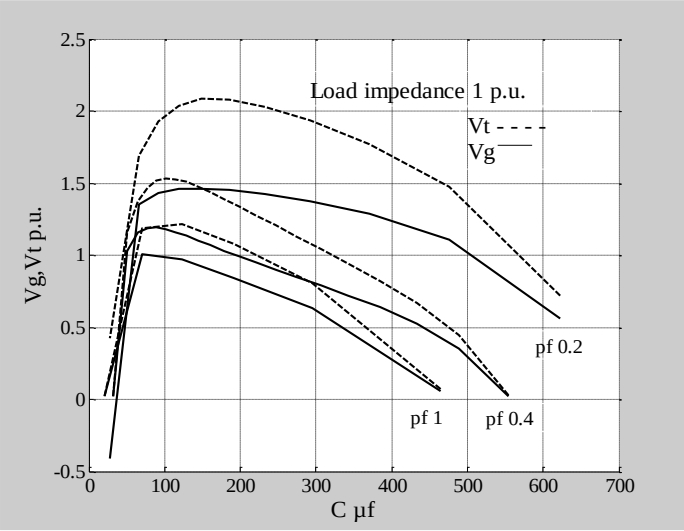

Figure 17 Variation of Vg and Vt for different power factors of load

Maximum V_t and V_g occurs almost for the same capacitor value. It is obvious to get increasing value of capacitor if power factor reduces because inductive reactance of load increases for lower power factor and to compensate it, capacitor value needs to be increased. Control of terminal voltage is possible by controlling the capacitor current. Capacitors can be connected to the motor windings either in star or in the delta. Other types of connections are possible but performance is poor.

V. DESIGN OF WATER WHEEL:

A water wheel is used as a prime mover in this project. Water wheels were used in the past for doing mechanical work. With the advent of turbines, the water wheels became obsolete. But once again the water wheel is revived for electrical power generation applications especially for rural areas [8]. For water flow of low head of less than 5 meters, water wheel is the best choice. While designing the water wheel, the available effective head of water, its discharge and power to be developed is taken into consideration. Fig. 18 shows the test site.

Fig. 18 Check dam site.

The approximate power that can be developed by a water wheel is given by [9].

$$P = QH_g\gamma\eta_w \quad (19)$$

Where

P is the power developed in kilowatts.

Q is the flow rate or discharge of water in m^3/ sec

H_g = Effective head of water (m)

γ is the specific weight of water 9.81 KN / m^3

η_w = efficiency of the water wheel

The water wheel is coupled to the generator through pulleys and belts to adjust the speed of the generator. The efficiency of the mechanical parts and the generator should also be accounted for while calculating the output power. Hence, equation (19) is modified as

$$P = QH_g\gamma\eta_w\eta_m\eta_g \quad (20)$$

Where

η_m = efficiency of mechanical parts

η_g = efficiency of the generator

Diameter of water wheel is inversely related to the speed. Water wheels with large diameters run very slowly. Length of water wheel affects the total power developed by the wheel. Long water wheels have higher torque than short water wheels. Fig. 19 shows variation of speed with diameter of wheel for different water heads. Fig. 20 shows Power developed Vs width of water wheel.

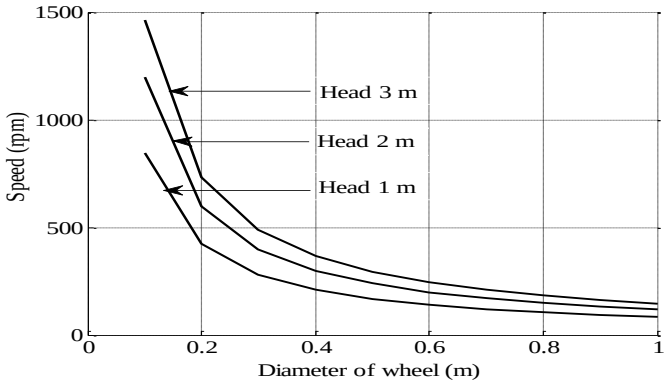

Fig. 19 Speed Vs diameter of water wheel

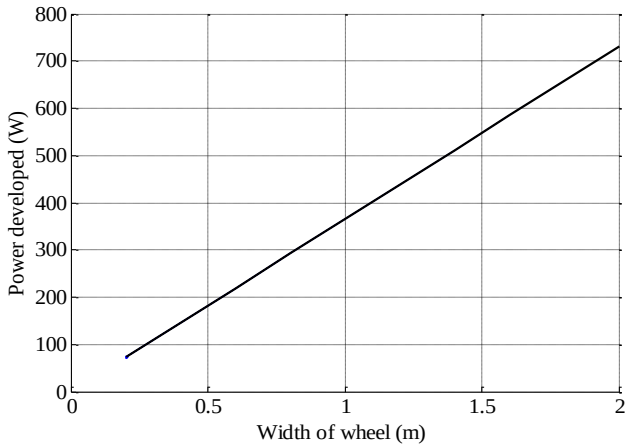

Fig. 20 Power developed Vs width of water wheel

Data obtained from the state irrigation department shows that water discharge from the site is 650 liters per second for a width of 3.05 meters. The effective head was measured as 1 meter. The efficiency of the generator estimated from laboratory tests is 60% and that of the mechanical system is assumed as 60 % so that the combined efficiency is 36% say 35%. Efficiency of the water wheel in the past was around 30 % but with new developments in the material and technology, it may be as high as 70 %. For this project water wheel efficiency is assumed as 50 % [10]. Target output of 200 watts was chosen. The incident water flow required for 200 watts output is calculated from (20).

$$200 * 10^{-3} = Q * 1 * 9.81 * 0.5 * 0.35$$
$$\therefore Q \approx 0.116\, m^3/\text{s}$$
$$or\ Q = 116\, l/s \qquad (21)$$

Width of water wheel required for this incident flow is given by

$$W = (116/650) * 3.05 = 0.544\, m$$

With required clearances the width of the wheel is chosen as 620 mm. Velocity of falling water is given by

$$V = \sqrt{H_g * 2g} \qquad (22)$$

Where V = velocity of falling water in m/s.
H_g = Effective head of water (m)
g = gravitational constant 9.81 m/s^2

$$V = \sqrt{(1 * 2 * 9.81)}$$
$$= 4.43\, m/s$$

For fabricating the wheel, two circular wooden plates of 760 mm diameter are used. Six vanes are formed by cutting a 300 mm diameter PVC pipe in two halves. A mild steel shaft of diameter 25 mm and length 1200 mm is used to support the wooden plates. Wooden plates are applied with oil paint to prevent erosion by water. Vanes are fitted to the wooden plate as shown in Fig. 21. Assembled water wheel is shown in Fig. 22.

.

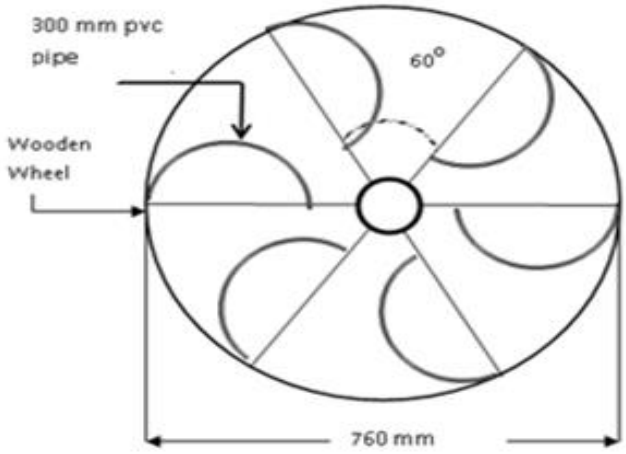

Fig. 21 Water wheel template

Fig. 22 Water wheel Fabricated by authors

To calculate the speed of water wheel,

$$Circumference\ of\ the\ wheel = \pi(Diameter\ of\ wheel)$$
$$= 2.38 \text{ meters} \qquad (23)$$

From the velocity of water and the circumference of the water wheel, the number of revolutions of the water wheel can be calculated.

$$No.\ of\ revolutions = \frac{4.43}{2.38} * 60$$
$$\approx 112\, rpm \qquad (24)$$

Actual speed checked at the site was 110 rpm. It was increased in two steps by using four pulleys. Fig. 23 shows the complete assembly. Two lamps of 100 watts were connected as load. The system worked properly.

Fig. 23 Complete setup of the Pico Hydro unit

Delta connected excitation capacitors of 20 µf each were connected to the generator cable along with the lamps. The system supplies 200 watts at 220 volts. The speed was observed to drop drastically when loading was increased. Load test readings at the actual site are shown in table -7.

Table 7 Load and speed readings of SEIG at site

Speed (RPM)	Terminal voltage (V)	Output power (W)
1200	240	100
1100	220	200

For the selected width of the water wheel, actual discharge is calculated from (19) as

$$Q = \frac{0.62 \times 650}{3.05} = 132.13 \text{ l/s}$$

$$Overall\ efficiency\ of\ the\ unit = \frac{200}{132.13 \times 9.81 \times 1} \times 100 = 15.43\ \%$$

Efficiency of the water wheel can be approximately calculated as

$$Overall\ efficiency = \eta_w * \eta_g * \eta_m$$

Where generator efficiency is 60% and mechanical efficiency is assumed as 60%.

$$\therefore\ \eta_w = 42.86\ \%$$

There is further scope for improving the efficiency by improving the mechanical system and using an induction motor with higher efficiency.

VI. CONCLUSION:

Laboratory tests for parameter extraction of equivalent circuit were conducted and the data is used for MATLAB steady state and dynamic analysis. No load generation tests and steady state analysis revealed that the value of excitation capacitor decides the overall loading capacity of the machine, the speed at which the generation will start and loading of the prime mover. Excitation capacitors also decide the peak voltage the machine would generate. When over loaded, the generation stops without any side effects. Frequency of the generated supply is important and it depends on the speed. Low value of excitation capacitor requires higher speed for generation so that the frequency can be close to the rated value.

Design and fabrication procedure of a water wheel is explained. Designed output is obtained from the unit. Results of laboratory and field tests conducted on a induction motor in SEIG mode are presented. MATLAB simulation results have also been presented and they corroborate the field and lab test results.

VI. REFERENCES:

1) Kharisma S. Gautama, Dimas Agil Triatmojo, Fitrian Pambudi, Doni Yusdinar, Karina Asrimaya, Rizaldy Azhar, Mohammad Ikhsan, "*Palapa - Distributed power generation for the development of underdeveloped villages in Indonesia"*, International conference on electrical engineering and informatics. 17-19 July 2011, Bandung, Indonesia, IEEE.
2) H. Zainuddin, M. S. Yahaya, J. M. Lazi, M. F. M. Basar, Z. Ibrahim, *"Design and development of Pico-Hydro generation system for energy storage using consuming water distributed to houses*", World Academy of Science, Engineering and Technology.59, 2009, pp 154-159
3) Haval Sardar Kamil, S. U. Kulkarni, "*Overview of wind turbine driven self-excited induction generator*", International Journal of Innovative Technology and Exploring Engineering (IJITEE) ISSN: 2278-3075, 2013, Volume-2, Issue-4.
4) Milan Radic, Zoran Stajic, Dusan Arnautovic, "*Critical speed capacitance requirements for self-excited induction generator",* Automatic control and robotics, Vol. 8, No 1, 2009, pp. 165 - 172.
5) Theodore Wildi, "*Electrical machines, drives and power systems"*, Fifth edition, Prentice Hall, 2002
6) Ofualagba, G and Ubeku, E. U., "*The analysis and modeling of a self-excited induction generator driven by a variable speed wind turbine"*, Fundamental and Advanced Topics in Wind Power, Dr. Rupp Carriveau (Ed.), ISBN: 978-953-307-508-2, In Tech, 2011, pp 249-268.
7) S. S. Katre, A. C. Joshi, Dr. V. N. Bapat, "*Effect of excitation capacitor on the performance of a self-excited induction generator",* International journal of emerging technologies and applications in engineering, technology and sciences, ISSN: 0974 - 3588, 2010, Volume 3, Issue 1, pp 722- 725.
8) G. Akhyar Ibrahim, C. H. Che Haron, C. Husna Azhari, "*Traditional water wheels as a renewable rural energy*", The Online Journal on Power and Energy Engineering (OJPEE), 2014, Vol. 1, No. 2, pp 62-66.
9) Rudy Behrens, "*Design calculations for overshot waterwheels*", Backwoods Home Magazine Issue,18,1990
10) Emanuele Quaranta, Stefano Fontan, Paolo Cavagnero, Roberto Revelli," *Efficiency of traditional water wheels*", E-proceedings of the 36th IAHR World Congress 28 June - 3 July, 2015, The Hague, the Netherlands, pp. 1-4.